Scattering, Trapping, and Ionization of HCl at the Surface of Liquid Glycerol

Ilya Chorny and Ilan Benjamin*

Department of Chemistry, University of California, Santa Cruz, California 95064

Gilbert M. Nathanson*

Department of Chemistry, University of Wisconsin, Madison, Wisconsin 53706

Received: June 26, 2003; In Final Form: October 22, 2003

A model for the interactions between HCl and liquid glycerol, based on the Empirical Valence Bond (EVB) approach, is developed and used to investigate by molecular dynamics computer simulations the early events following the collision of an HCl molecule with the glycerol surface. The calculated trapping probability at 2.4 and 22 kcal/mol collision energies and the fractional energy loss of scattered HCl molecules agree well with experiments. The potential of mean force for HCl in the bulk and at the glycerol surface exhibits a low barrier to the formation of the contact ion pair, suggesting the possibility of proton transfer at the interface. Trapped HCl molecules undergo rapid relaxation and solvation and begin to form contact ion pairs on the picosecond time scale, which is consistent with the low barrier to the formation of the ion pair derived from the equilibrium potential of mean force calculations.

I. Introduction

Understanding the nature of the interactions between an acid molecule and a polar solvent is one of the fundamental problems in chemistry.[1−11] A key step in bringing the solute and solvent together is the transfer of the acid molecule from the gas phase through the liquid surface region and into the bulk liquid.[12−15] Besides the fundamental interest in elucidating the role of the surface region on the rate of this process,[16] the uptake of gaseous acids by water surfaces has important environmental[17] and industrial implications.[18]

Studies in bulk liquids have shown that ionization of an acid molecule by a condensed phase environment is thermodynamically driven by the solvation of the ionic products.[19] The solvent also plays an important dynamic role as its reorganization provides the low barrier for the proton transfer.[4,6] Numerous theoretical and experimental studies of the behavior of HCl at the surface of ice have shown that HCl ionizes when it is embedded within the first layer of ice molecules[20] or if it is located on top of the ice surface and there are free OH groups present at the surface.[9,12,10] These results are consistent with other studies that demonstrate that a small cluster of water molecules is sufficient to support the ionization process.[11,22] There is also indirect evidence for the existence of ionized HCl molecules at water surfaces. Sum frequency generation experiments, for example, were unable to detect molecular HCl at aqueous surfaces.[23,24]

The possibility of interfacial acid dissociation and interfacial proton transfer can be examined by molecular beam scattering of HCl and DCl from the surface of the polar, low vapor pressure liquid glycerol.[13,14] These experiments have helped to develop a detailed picture of the uptake of HCl into glycerol by unraveling the roles played by the interfacial region on the elementary processes of scattering, trapping, dissociation, and recombination. In particular, recent scattering experiments utilizing both HCl and DCl showed that, at an approach angle of 45°, the HCl trapping probability exceeds 0.9 and 0.6 at incident energies of 2.4 and 22 kcal/mol. When DCl is directed at glycerol, 20% of the molecules momentarily trapped at the surface desorb back into the gas phase before D → H exchange can occur. The most surprising observation is that 7% of the trapped DCl molecules undergo D → H exchange and desorb as HCl within 1 μs, implying that DCl dissociation and HCl recombination occur at or just below the glycerol surface. The remaining 73% of the trapped DCl molecules diffuse deeply as ions within the bulk liquid, slowly evaporating as HCl.

The purpose of this paper is to develop a potential energy surface that can describe the scattering and trapping of HCl at the glycerol surface, provide molecular insight into the mechanism of trapping, and examine the possibility of ionic dissociation at the interface region. We use the Empirical Valence Bond (EVB) approach, which has been extensively employed,[1,6,7] to study similar systems in which strongly coupled ionic and covalent states give rise to a system confined to move on an adiabatic ground-state surface. We should point out that the model we have developed is incapable of describing the later stages of proton transfer among the glycerol molecules. This process involves the development of a separate model similar to those recently used to study proton transfer in water.[6,7]

The rest of this paper is organized as follows. In section II we describe the EVB model and the potential energy surfaces used. In section III we present the results of the potential of mean force calculations and the scattering trajectories. Our conclusions are summarized in section IV.

II. Potential Energy Functions

Designing a realistic potential energy function to model the interaction between the HCl and the glycerol molecules is a challenging problem. The relatively large number of solvent molecules needed for describing the surface and the bulk region limits the treatment to a classical one. The difficulty is in developing a unified classical Hamiltonian that can accurately describe both the scattering of the mostly covalent HCl from

10.1021/jp035825k CCC: $27.50
Published on Web 12/13/2003

the surface and the trapping of HCl followed by dissociation to H^+ and Cl^- ions. While the treatment of the transition from the covalent to the ionic form can be satisfactorily accomplished by the Empirical Valence Bond (EVB) method, the subsequent proton transfer and exchange requires a much greater effort involving a quantum description of HCl in a cluster of glycerol molecules. This later approach recently has been used to study the dissociation of HCl in water starting from a hydrated-HCl configuration.[6,7] We postpone issues related to the proton transfer and proton exchange in the HCl/glycerol cluster to a future publication and concentrate in this paper on the early steps of HCl scattering, trapping, and dissociation to a contact ion pair. Our goal is to develop a practical model potential that is capable of capturing the important physical features of the system, without making it computationally impractical. Our first attempt to model this complex system is described below.

A. The Valence Bond Model. The dynamics of the system are described by using an empirical two-state (ionic and covalent) valence bond model[1]

$$\psi = c_{\mathrm{cov}}\psi_{\mathrm{cov}} + c_{\mathrm{ion}}\psi_{\mathrm{ion}} \tag{1}$$

The electronic ground-state energy in the adiabatic approximation as a function of all nuclear coordinates can be obtained by diagonalization of the total Hamiltonian. This gives an adiabatic Hamiltonian suitable for describing the classical motion of the system in the ground state in the form:

$$H_{\mathrm{ad}} = E_{\mathrm{k}} + U_{\mathrm{ad}};$$
$$U_{\mathrm{ad}} = \frac{1}{2}(U_{\mathrm{cov}} + U_{\mathrm{ion}}) - \frac{1}{2}[(U_{\mathrm{cov}} - U_{\mathrm{ion}})^2 + 4U_{\mathrm{coup}}{}^2]^{1/2} \tag{2}$$

where we assume that $\psi = (\psi_{\mathrm{cov}},\psi_{\mathrm{ion}})$ is an orthonormal basis. U_{cov} includes the gas-phase Morse potential for the HCl molecule, the interaction of HCl with the solvent molecules modeled as Lennard-Jones plus Coulomb terms, and the solvent intermolecular and intramolecular potentials:

$$U_{\mathrm{cov}} = U_{\mathrm{Morse}}(R) + U_{\mathrm{HCl-Gly}} + U_{\mathrm{Gly}} \tag{3}$$

U_{ion} includes the gas-phase HCl ionic potential, the interaction between the two ions and the solvent, and the energy offset relative to the covalent state. The solvent intermolecular and intramolecular terms are unchanged:

$$U_{\mathrm{ion}} = U_{\mathrm{H^+Cl^-}}(R) + U_{\mathrm{H^+Cl^-\!-Gly}} + U_{\mathrm{Gly}} + \Delta \tag{4}$$

U_{coup} is a fixed electronic coupling (35 kcal/mol) whose value is selected (together with other parameters in the energy offset term Δ) to reproduce experimental data as discussed below. We now discuss the different terms in detail.

B. Liquid Potential Energy Functions. As mentioned above we assume (as typically done with EVB models in liquids) that the liquid potential energy function U_{Gly} is the same in the two diabatic states. The model we use for glycerol has been described in detail elsewhere[25,26]and we give here a brief summary. (For other molecular models of glycerol see refs 27−30.) Each glycerol molecule is represented by a nine-site flexible model in which the CH and the two CH_2 groups are described using a united atom representation, but the oxygen and hydrogen atoms in the three hydroxyl groups are treated explicitly. The glycerol intramolecular potential energy function is represented by a sum of harmonic bond stretching and angle bending vibrations and of standard proper and improper torsional terms. The parameters are taken from the Amber force field[31] and are given elsewhere.[25] The glycerol intermolecular potential energy function is represented by a pairwise additive sum of Lennard-Jones plus Coulomb terms (LJC) over all pairs of sites:

$$U_{\mathrm{Gly}} = U_{\mathrm{LJC}} = \sum_{i<j} 4\epsilon_{ij}\left[\left(\frac{\sigma_{ij}}{r_{ij}}\right)^{12} - \left(\frac{\sigma_{ij}}{r_{ij}}\right)^{6}\right] + \frac{q_i q_j}{r_{ij}} \tag{5}$$

where r_{ij} is the distance between sites i and j which are in two different molecules, q_i and q_j are the fixed charges on sites i and j, respectively, and the Lennard-Jones parameters σ_{ij} and ϵ_{ij} are determined from the parameters of the individual sites according to the usual combination rules for mixtures:[32]

$$\sigma_{ij} = (\sigma_{ii} + \sigma_{jj})/2; \quad \epsilon_{ij} = (\epsilon_{ii}\epsilon_{jj})^{1/2} \tag{6}$$

The glycerol LJC parameters for the individual sites have been determined by a variety of methods and are given elsewhere.[25] Several properties of the bulk liquid and the surface calculated with these potentials are in reasonable agreement with experiments.[33] The calculated density is 1.23 ± 0.02 g/cm^3 (experiment: 1.26 g/cm^3 at 293 K). The calculated enthalpy of vaporization is 73 ± 2 kJ/mol (experiment: 88 kJ/mol at 328 K). The calculated surface tension is 58 ± 1 dyn/cm (experiment: 63.4 dyn/cm at 293 K).

C. The HCl and the HCl−Glycerol Potentials. The gas-phase Morse potential for HCl in eq 3 is

$$U_{\mathrm{Morse}}(R) = D_{\mathrm{e}}[e^{-2a(R-R_{\mathrm{eq}})} - 2e^{-a(R-R_{\mathrm{eq}})}] \tag{7}$$

whose parameters are taken from Herzberg[34] and given in Table 1. The gas-phase HCl potential for the ionic diabatic state (first term on the right of eq 4) is given by the Coulomb attraction between H^+ and Cl^- plus a Lennard-Jones term, which provides the short-range core repulsion between the two ions:

$$U_{\mathrm{H^+Cl^-}}(R) = \frac{-1}{R} + 4\epsilon_{\mathrm{HCl}}\left[\left(\frac{\sigma_{\mathrm{HCl}}}{R}\right)^{12} - \left(\frac{\sigma_{\mathrm{HCl}}}{R}\right)^{6}\right] \tag{8}$$

The Lennard-Jones parameters in this term are given in Table 1 for the individual H and Cl sites from which the σ_{HCl} and ϵ_{HCl} are determined, using the combination rule (eq 6).

The interactions between the covalent HCl and the glycerol molecules ($U_{\mathrm{HCl-Gly}}$ in eq 3) as well as the interactions between the ion pair H^+Cl^- and the glycerol (middle term in the right side of eq 4) are modeled by LJC potentials with different sets of parameters given in Table 1. Note, however, that the Coulomb interactions between the covalent HCl and the glycerol molecules are modeled by using a three-point charge model for HCl. In addition to the two charges localized on the H and Cl atoms, a third charge (q_3) is located at a distance 1.00 au (0.529Å) away from the Cl atom on the line connecting the H and Cl atoms. The three charges and the location of the third charge were selected to reproduce the large quadrupole moment of HCl.[35]

D. The Energy Offset Term. An additional term Δ is added to the ionic state and represents the "gas-phase shift", which is the difference in energy between the two diabatic states as a

TABLE 1: Potential Energy Parameters

D_{e} (kcal/mol)	103.25	q(covalent Cl)	−0.909
R_{eq} (Å)	1.275	q_3(covalent)	0.403
a (Å^{-1})	1.325	q(ionic H)	+1
σ_{H} (Å)	1.5	q(ionic Cl)	−1
ϵ_{H} (kcal/mol)	0.039	Δ_∞ (kcal/mol)	230.16
σ_{Cl} (Å)	4.0	α	0.46
ϵ_{Cl} (kcal/mol)	0.348	γ (Å^{-1})	0.005
q (covalent H)	0.506	U_{coup} (kcal/mol)	35

function of the HCl separation in the gas phase.

$$\Delta = \Delta_\infty(1 - \alpha e^{-\gamma R}) \quad (9)$$

The parameters α, γ, and Δ_∞ in eq 9 as well as the electronic coupling term are obtained by fitting to experimentally determined thermodynamic data for the dissociation of HCl to H^+ and Cl^- in glycerol and are listed in Table 1. Note that at large bond distances, Δ reduces to Δ_∞, which is the ionization energy of the hydrogen atom plus the electron affinity of the chlorine atom. At short bond distances, Δ allows us to lower the energy of the ionic curve (relative to the energy in infinite separation) to account approximately for stabilization of the ion pair by proton delocalization over several glycerol molecules. This approach can be shown to be equivalent to introducing an exponential electronic coupling term with a maximum value at the crossing region between the ionic and covalent diabatic states.

III. Results and Discussion

The results discussed below involve both equilibrium determination of the HCl potential of mean force (or the free energy profile) calculated in the bulk and the surface of glycerol and nonequilibrium scattering trajectories. We provide details about the methodology used in the appropriate places before describing the results.

A. Free Energy Profile for HCl Dissociation. The thermodynamics (and to some degree the dynamics) of the $HCl \rightarrow H^+ + Cl^-$ reaction in glycerol can be conveniently discussed in terms of the free energy of the system as a function of the HCl bond length *R*. There are several ways to compute this function and we chose to use the thermodynamic perturbation approach.[36,37] The free energy difference between any two HCl configurations can be written as:

$$\Delta A_{i\rightarrow j} = -kT \ln\langle \exp\{-[H(R_j) - H(R_i)]/kT\}\rangle_i \quad (10)$$

where $\langle ... \rangle_i$ is the ensemble average with the HCl interatomic distance *R* fixed at R_i. This method has been used to compute the free energy profile for the neutral solutes and ions in a large number of bulk and interfacial systems.[38−40]

The set of all $\Delta A_{i\rightarrow j}$ gives the potential of mean force (PMF) as a function of the HCl bond length *R* and it is computed in both the bulk and surface glycerol. For each configuration, 50 independent trajectories of 20 ps each are run, each with a different fixed HCl bond distance. The PMF at the interface and in the bulk and the intramolecular potential energy functions for the two diabatic states are shown in Figure 1. The free energy profile can be thought of as the solvent-modified intramolecular potential energy surface for HCl. In the gas phase, the ionic and the covalent curves do not cross, but in the condensed phase, the ionic curve is lowered due to the stabilization of the ions by the polar solvent. When the ions are fully separated, the stabilization is approximately equal to the sum of the solvation free energies of the H^+ and Cl^- ions. At shorter HCl distances, the PMF is dominated by the covalent state as represented by the first minimum. This minimum is approximately at the same energy value in the gas phase and in the bulk, since a separate estimate of the free energy change for the process HCl(gas) → HCl(solution) gives 0.5 ± 0.5 kcal/mol. As the bond distance increases, stabilization of the ionic state by solvent glycerol gives rise to the second minimum, which we identify as a contact ion pair. The dissociation free energy is −6 ± 0.5 kcal/mol in bulk glycerol compared with −2 ± 0.5 kcal/mol at the interface. The bulk value is close to the experimental result of −4.5 ± 0.7 kcal/mol.[13] The formation of a contact ion pair in the bulk and at the interface involves a barrier of 2 kcal/mol, which is consistent with the expected rapid dissociation of HCl in highly polar solvents. While our potentials can be used to compute the potential of mean force beyond the 2 Å bond separation, it is likely not to be relevant to the problem of proton transfer and exchange. Recent calculations of HCl ionization in water[4,6,7] clearly demonstrate that delocalization of the proton on several solvent molecules is important and the relevant reaction coordinate involves significant solvent reorganization.[4,6] Thus, the large barrier (for both interface and bulk) for the separation of the contact ion pair suggested by the PMF in Figure 1 should be significantly reduced when proton exchange with neighboring glycerol molecules is taken into account. It is not clear how to incorporate this issue in a model that also describes the scattering of HCl, and this problem is left for a separate study.

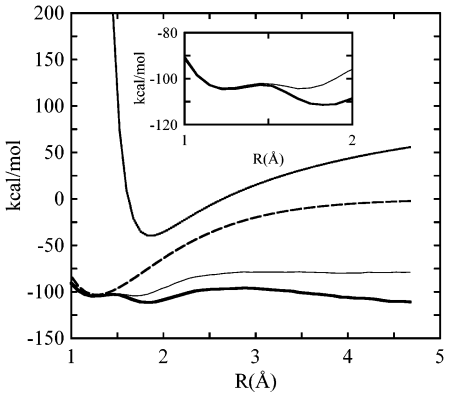

Figure 1. The free energy profile of HCl in bulk glycerol (thick solid line), at the interface (thin solid line), and the potential energy surfaces for the covalent (dashed line) and ionic (dotted line) states in the gas phase. The insert shows the potential of mean force in the contact ion pair region.

B. Scattering of HCl Off the Surface of Glycerol. As a prelude for a discussion of the scattering results, we first briefly describe the glycerol surface region. If one adopts the normal definition of a liquid surface "region" as the region over which the average density changes from 90% to 10% of the bulk liquid density, then for glycerol this is a narrow slab about 4 Å thick. The sharp transition from the bulk liquid to bulk vapor is quite rough on a local scale. This local roughness is the result of protrusions made of one or two glycerol molecules and is also characterized by a relatively wide distribution of local energy minima for the adsorption of a solute molecule. The top surface layer is comprised of 40% hydroxyl hydrogens, 40% CH and CH_2 groups, and 20% oxygen atoms.[25]

The scattering calculations are performed on a system that includes 343 glycerol molecules arranged in a lamella 44 Å thick in the perpendicular *Z* direction with an *X*,*Y* cross section of 34 Å × 34 Å. This creates two liquid/vapor interfaces along the *Z*-dimension. Both surfaces are used for the scattering calculations. The results from the two surfaces are folded together. Periodic boundary conditions are applied in the *X* and *Y* dimensions.

Scattering events are simulated by initially placing the HCl at a distance larger than the 17 Å cutoff distance for the HCl−glycerol interactions. The HCl molecule is given an initial velocity corresponding to a specified collision energy E_i, directed toward the surface at an angle of 45° relative to the surface normal. Molecular dynamics calculations are carried out with two collision energies, 22 and 2.4 kcal/mol. These are the same collision energies used in the experiments of ref 13. Eight hundred trajectories are run with use of 80 different surface

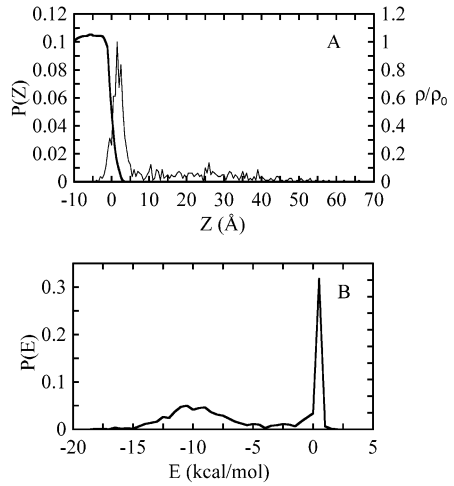

Figure 2. (A) The thin solid line is the distribution of final positions of HCl molecules along the interface normal (*Z* direction) at the end of the 5-ps trajectory. The thick solid line depicts the glycerol density profile. (B) The distribution of the HCl-GLY interaction energies (covalent component only) at the end of the 5-ps trajectory.

configurations (thermalized at 300 K) for the 22 kcal/mol calculations and 260 trajectories are run with use of 26 different surfaces for the 2.4 kcal/mol calculations. For each surface, the different trajectories correspond to different initial positions in the *X*,*Y* plane and different thermal velocities in all degrees of freedom other than the HCl translation. These velocities are sampled from a Maxwell−Boltzman distribution at 300 K. In each trajectory, it takes ≈1 ps for the 22 kcal/mol and ≈3 ps for the 2.4 kcal/mol HCl to collide with the surface. The trajectory is then followed for a total of 5 ps for the 22 kcal/mol HCl and 10 ps for the 2.4 kcal/mol HCl. We chose 5 ps for the 22 kcal/mol trajectories because preliminary simulations showed that this time is sufficient for those trajectories that get trapped at the surface to thermalize. We ran the 2.4 kcal/mol trajectories for 10 ps because it took longer for them to reach the surface. Each trajectory is analyzed to extract information about the final energy distribution of the trapped and scattered atoms, the trajectory history of the colliding atoms, and energy flow into the liquid. We note that none of the liquid surfaces used in the simulations have glycerol in the "vapor" phase. This guarantees that the HCl molecule scatters from the liquid surface itself, thus corresponding to the experimental situation of very low vapor pressure (10^{-4} Torr at 300 K).

C. Trapping of HCl. An HCl molecule colliding with the surface may be reflected after one or multiple collisions with the surface, or it may reach thermal equilibrium with the surface and stay trapped on the time scale of our simulation. The simulation of 2.4 kcal/mol HCl showed 96% trapping of the colliding HCl molecules, in excellent agreement with the 92% value obtained experimentally. The number of trajectories that lead to scattering from the surface was statistically insignificant and thus we limit our discussion here to the 22 kcal/mol trajectories because the behavior of the HCl molecule, once it is thermalized, is independent of collision energy.

The data in Figure 2 provide an overall summary of the outcome of the trajectories. Panels A and B are snapshots of the distribution of the HCl center of mass position and the distribution of the covalent HCl−glycerol interaction energy at the end of the 5-ps trajectory, respectively. Panel A also shows the density profile of glycerol (where the position *Z* refers to the position of the central carbon atom). The top surface glycerol atoms are located on average at 6 Å. The system reaches bulk

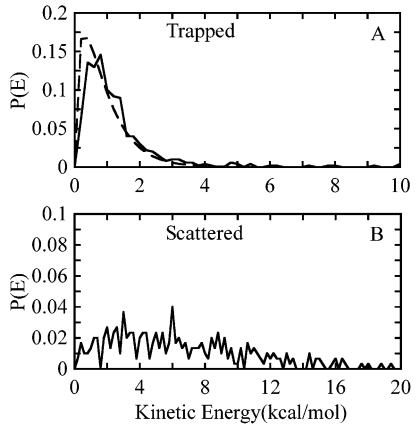

Figure 3. Final (end of 5-ps trajectory) translational energy distributions for HCl molecules that are trapped (A) and that scatter (B). The dashed line in panel A is a fit to a Boltzman distribution at the 300 K temperature of the liquid.

density at around −2 Å, where $Z = 0$ is positioned at the Gibbs dividing surface. The majority of HCl molecules end up with a *Z* position less than 6 Å and will be labeled as trapped whereas the HCl with *Z* positions greater than 6 Å will be labeled as scattered. The trapping probability is 64% and is in excellent agreement with experimental value of 63%. Panel B is consistent with panel A in that the interaction energy of the 36% of the trajectories that lead to scattering is near zero. Note also the wide distribution of negative interaction energies. This reflects the wide range of trapping sites on the surface as well as the very different ionic character of the HCl molecules at the end of the 5-ps trajectories, as will be discussed below.

D. Kinetic Energy Distributions and Energy Loss of Scattered HCl. The translational energy distribution of the trapped HCl molecules at the end of the 5-ps trajectory is depicted in Figure 3A. The distribution of trapped trajectories is fit nicely by a Boltzman distribution at the 300 K temperature of the liquid. This is consistent with the notion that the HCl molecules that get trapped at the surface thermalize within 5 ps.

The energy distribution for the HCl molecules that scatter from the surface is depicted in Figure 3B. The average fractional energy transfer defined as $(E_i - \langle E_f \rangle)/E_i$, where E_f and E_i are the final and initial translational energies of HCl, is 0.69 and is in excellent agreement with the experimental value of 0.70 at 22 kcal/mol.[13,14]

It is of interest to examine to what degree the fractional energy loss of scattered HCl molecules fits a simple kinematic model. Consider a collision between a hard sphere gas atom and a hard sphere surface atom in the presence of a square well potential of depth *V*. The fractional energy loss for such a collision is determined by the ratio of the gas to surface masses $\mu = m_g/m_s$, the deflection angle χ (equal to $180° - \theta_i - \theta_f$), the well depth *V*, and the initial energy E_i of the colliding gas molecule and is given by:[41,42]

$$\frac{\Delta E}{E_i} = \frac{2\mu}{(1+\mu)^2}[1 - \cos\chi((1 - \mu^2 \sin^2\chi)^{1/2} + \mu \sin^2\chi](1 + V/E_i) \quad (11)$$

To apply this relation we take $V = 0$ because the HCl molecule approaches the surface with a random orientation, giving rise to a distribution of interaction energies which averages out to near zero (in part because the H or the Cl pointing down correspond to opposite signs of the electrostatic energy, which

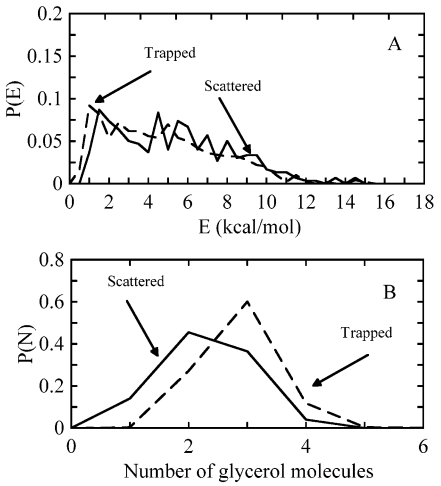

Figure 4. (A) The distribution of the HCl−glycerol maximum interaction energy for HCl molecules that are trapped (dashed line) and that scatter (solid line). (B) The fraction of trajectories that experience a repulsive collision with the indicated number of glycerol molecules for trapped (dashed line) and scattered (solid line) HCl molecules.

will be confirmed below when we examine the time-dependent ensemble average of the HCl−glycerol interaction energy). We take $\chi = 76.4°$, which is the average value obtained from the molecular dynamics trajectories. With this value we can reproduce the fractional energy loss if we set the surface "atom" mass to 54 amu. This is approximately the mass of $^2/_3$ of a glycerol molecule, suggesting that the collision is localized around 2 of the 3 "backbone" carbon atoms. One should keep in mind that this is a very crude model that should not be pushed too hard (see ref 43 for a more sophisticated treatment). Because of the large collision energy relative to glycerol's torsional barriers, the actual collision dynamics must involve translation and conformational distortion of the glycerol molecule hit by the HCl, as well as energy flow to neighboring glycerol molecules.

E. Energy Flow Into the Liquid. One of the major issues in gas−liquid collision dynamics is identification of the mechanisms responsible for trapping or scattering of the colliding molecules. This is a difficult problem to resolve experimentally but can be addressed by using the molecular model developed here. With such large, 22 kcal/mol collision energies used in the experiment, the outcome of the collision should be determined mostly by the short-ranged repulsive Lennard-Jones forces. We consider a glycerol molecule as a participant in a "repulsive" collision if the interaction energy between the colliding HCl molecule and a surface glycerol molecule is positive at any given time during the trajectory. The "interaction energy" in this definition refers to the covalent term $U_{\mathrm{HCl-Gly}}$ in eq 3, since during the collision the HCl covalent character c_{cov}^2 is very close to 1.0. With this definition we find that in all of the trajectories, at least one glycerol molecule participates in a repulsive collision with a colliding HCl molecule, but in the majority of the trajectories the HCl is involved in more than one repulsive collision.

Figure 4A is the distribution of the maximum HCl−glycerol interaction energy for the HCl molecules that scatter and for those that get trapped at the surface. The distributions look very similar with an average positive interaction energy of 4.4 kcal/mol for the trapped and 5.0 kcal/mol for the scattered HCl. Figure 4B shows the fraction of trajectories as a function of the maximum instantaneous number of glycerol molecules participating in a repulsive collision with the HCl molecule.

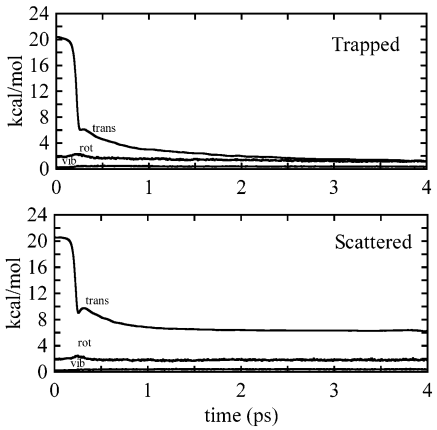

Figure 5. Ensemble average of the translational (trans), vibrational (vib), and rotational (rot) kinetic energy as a function of time for trajectories which get trapped (A) and which scatter (B).

The majority of the HCl molecules that scatter from the surface are involved in a repulsive collision with one or two glycerol molecules, while the majority of the molecules that get trapped are involved in a repulsive collision with two or more glycerol molecules. An identical result was obtained in previous studies of Ne and H_2O scattering off the surface of glycerol.[25,26] Thus, while all of the HCl molecules collide with the surface with essentially the same translational energy, the molecules that scatter were involved in a more localized collision as depicted by the fewer number of glycerol molecules repulsively interacting with the HCl.

Additional information about the dynamics of the energy exchange can be obtained by examining time-dependent ensemble averages of the different energy terms. Figure 5 shows the ensemble average of the translational, vibrational, and rotational kinetic energy of HCl as a function of time for trapped (A) and scattered (B) trajectories. Since different HCl molecules collide with the surface at different times due to surface corrugation, the averaging is done by aligning the trajectories such that $t = 0$ in Figure 5 corresponds to a point in time that is 250 fs prior to the collision with the surface. (A collision is defined as the point at which the translational velocity changes sign in either the *X* or *Z* direction.) Thus, the first minimum of the translational energy curve at $t = 250$ fs corresponds to the first collision. The sharp decay in the translational energy prior to hitting the surface reflects the fact that the HCl molecule climbs a repulsive wall prior to a change in the direction of its translation motion. We note that the HCl molecules that scatter have a smaller repulsive wall to climb. This is consistent with the facts mentioned earlier (Figure 4), namely that they interact with fewer molecules/atoms and thus lose less translational energy. Both the scattered and the trapped HCl molecules get rotationally excited following the collision due to the torque applied by the corrugated surface on the incoming HCl molecule. In contrast, the vibrational kinetic energy is unaffected by the collision. The translational and rotational excitations relax to thermal values within 4 ps if the HCl molecules are trapped whereas the scattered HCl plateau to their final average value upon leaving the surface.

Figure 6 shows the covalent component of HCl−glycerol interaction energy as a function of time for HCl that are trapped (thick line) and that are scattered (thin line). The averaging is done in the same way as Figure 5 where the maximum is the point in time in which the HCl molecule collides with the surface. The covalent component of the interaction energy prior to colliding with the surface is on average 1 kcal/mol less for

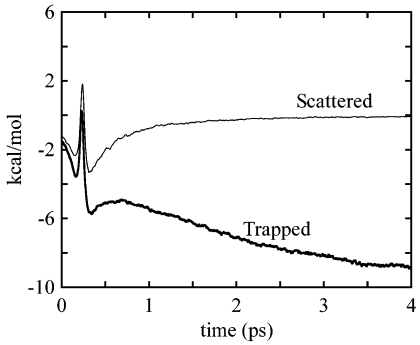

Figure 6. Ensemble average of the covalent component of the HCl−glycerol interaction energy as a function of time for molecules that are trapped (thick solid line) and that scatter (thin solid line).

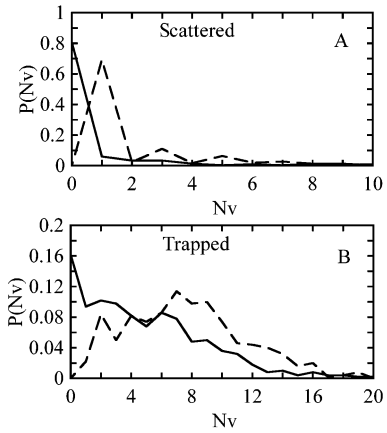

Figure 7. Distribution of the number of HCl translational velocity sign changes in the *X* (solid line) and *Z* (dashed line) directions for trajectories which scatter (A) and get trapped (B).

trapped than for scattered trajectories and this is consistent with the notion that trapped HCl molecules interact repulsively with more glycerol molecules/atoms (prior to being trapped). One should note that for HCl molecules that are trapped, the covalent component is a valid measure of the interaction with the liquid only for the early time events near the first collision. Beyond that time, the HCl molecule begins to dissociate and thus the interaction energy is a linear combination of both the covalent and ionic components. Thus, the data beyond the first collision are shown to provide a time scale for the stabilization of a trapped HCl molecule and do not convey the full stabilization with the liquid. The covalent component of the interaction energy plateaus to zero for HCl that scatter, as expected for molecules no longer interacting with the liquid molecules.

F. Trapping/Scattering Mechanism. To elucidate which factors lead to scattering or trapping, it is important to look at the behavior of the HCl molecule following the initial collision event. A useful method involves looking at the number of times the sign of the velocity vector changes in the *X* and *Z* dimensions. The *Y* dimension also can be followed but it is of little independent interest since all of the initial excitation is in the *XZ* plane. The number of sign changes is a measure of the number of consecutive collisions following the initial collision with the surface. Figure 7A depicts the fraction of HCl molecules that scatter as a function of the maximum number of velocity sign changes N_v. Most (70%) of the HCl that scatter do so after one sign change in the *Z* direction (dashed line) and no sign changes in the *X* direction (solid line). In fact, by examining the detailed correlation between the sign changes in the *X* and *Z* directions we find that 60% of the trajectories that

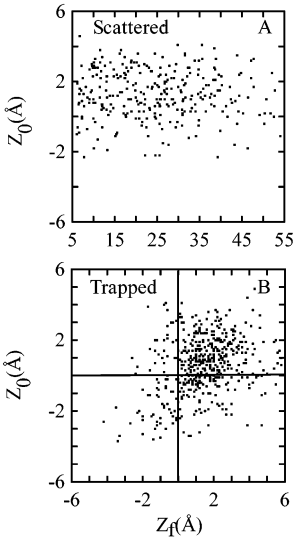

Figure 8. The *Z* position of the HCl molecule at the point of the first velocity sign change as a function of its *Z* position at the end of the 5-ps trajectory for trajectories which scatter (A) and get trapped (B). $Z = 0$ is the Gibbs surface.

undergo one sign change in the *Z* direction have no sign changes in *X* direction. The remaining 40% scatter with more than one velocity sign change in either the *X* or *Z* dimension. Thus, most of the HCl molecules that scatter do so ballistically and leave the surface in the forward direction. The even−odd alteration in Figure 7A is just an indication that the HCl leave the surface via the gas phase, so all the even values are zero.

Figure 7B shows the fraction of trajectories that lead to trapping as a function of the number of sign changes in the first 3 ps of the trajectory. The 3-ps value is chosen because this is the time it takes most of the HCl that scatter to leave the surface. As expected, the trajectories that lead to trapping undergo significantly more sign changes in both the *X* and *Z* dimension.

Figure 8 is a scatter plot depicting the correlation between the position at the time of the first velocity sign change (Z_0) and the final position of the HCl molecule at the end of the trajectory (Z_f) for HCl molecules that scatter (A) and for those that are trapped (B). The data in panel A show that HCl molecules scatter independently of where they hit the surface in the *Z* direction. What decides the fate of an HCl molecule is the local environment immediately after the collision, as was indicated by the data in Figure 6. On the other hand, Figure 7B demonstrates that the majority of the HCl molecules which enter the bulk ($Z_F < -2$ Å) do so ballistically (through a crevice) and not diffusively. This is as expected because thermal diffusion from the surface to the bulk should not be seen on the time scale of the simulation.

G. Contact Ion Pair Formation. When the HCl first interacts with the surface, its covalent character is nearly 100%. As is clear from the potential of mean force of Figure 1 (see in particular the insert), there is a small barrier between the covalent state near $R = 1.2$ Å and the contact ion pair near $R = 1.8$ Å (where the ionic character is nearly 100%). Thus, one expects a rapid increase in the fraction of ionic character as the HCl gets solvated by glycerol and the barrier is overcome. Figure 9 is a scatter plot of the fraction of the covalent character as a function of the HCl bond length at the end of the 5-ps trajectories. The solid curve shows for comparison the covalent character as a function of bond length for the HCl in equilibrium with the solvent. There is a significant population of HCl molecules that did not cross the barrier and their covalent

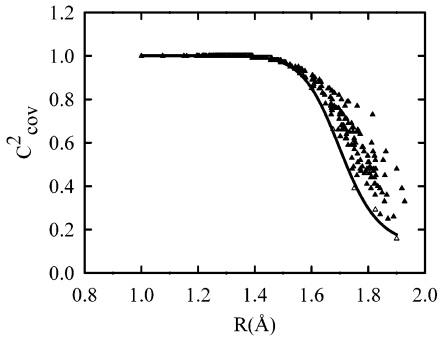

Figure 9. Scatter plot showing the fraction of the covalent component of the ground-state eigenvector as a function of the HCl bond length at the end of the trajectory. The solid line depicts the covalent character of HCl allowed to reach an equilibrium with the bulk liquid.

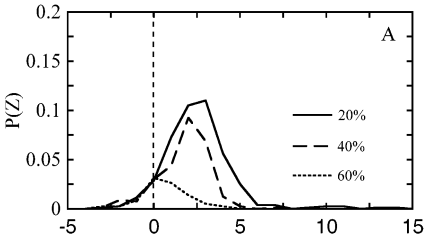

Figure 10. Distribution of the *Z* positions where the HCl molecule becomes 20% (solid line), 40% (dashed line), and 60% (dotted line) ionic. The distributions are normalized by the total number of trajectories.

character is near 100% (for example, 86% have a covalent character of 90% or higher.) However, quite a large number of HCl molecules that crossed the barrier still have mostly covalent character (note the number of points above the solid line in the region $R = 1.8$ Å). This reflects the slow solvation dynamics by the high viscosity glycerol liquid.

It is of interest to examine the correlation between the degree of dissociation (to ions) and the location of HCl along the surface normal. In Figure 10 the solid line represents the distribution of *Z* positions at the moment the HCl ionic character reached 20% for the first time within the 5-ps trajectory. The dashed and dotted lines correspond to the 40% and 60% ionic character, respectively. The curves are normalized by the total number of trajectories (which explains why the area under the three curves is different). The shift in the curves to lower values of *Z* as the ionic character increases suggests that the HCl is more likely to achieve a larger percentage of ionic character in the bulk than at the interface. The observation that HCl achieves significant ionic character within 5 ps, in conjunction with the free energy calculations in Figure 1 which show that ion pairing is thermodynamically stable in the interfacial region, suggests that the trapped HCl molecules are likely to form ion pairs at the interface before diffusing into the bulk. This ion pairing provides a rationale for the experimental observation that, in experiments utilizing DCl, 7% of the trapped DCl molecules undergo near-interfacial D → H exchange prior to leaving the surface within 1 μs as HCl. We hope to investigate the mechanism of this proton transfer in future studies.

We finally discuss some of the energetics and structural issues involved in the dissociation of HCl after the onset of trapping. Figure 11A shows the distribution of the HCl translational energy at the moment the ionic character reached 20% (solid line), 40% (dashed line), or 60% (dotted line). As expected, substantial relaxation of the HCl translational motion occurs before a significant increase in the ionic character is observed. All of the distributions in Figure 11A are shifted to smaller

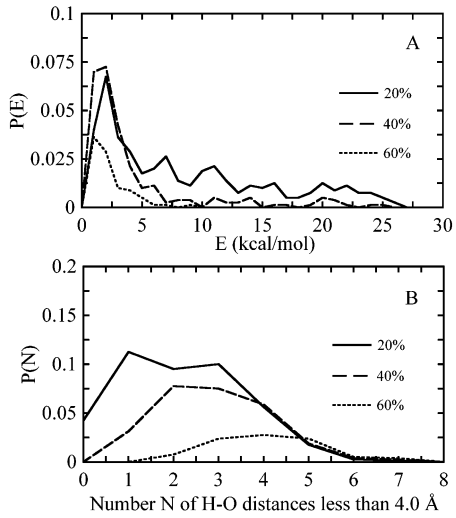

Figure 11. (A) Distribution of the translational energy when the HCl molecule becomes 20% (solid line), 40% (dashed line), and 60% (dotted line) ionic. (B) Distribution of the number of H−O distances less than 4.0 Å at the moment the HCl molecule becomes 20% (solid line), 40% (dashed line), and 60% (dotted line) ionic. The distributions are normalized by the total number of trajectories.

translational kinetic energies when compared with Figure 3B, which suggests that the HCl molecule must undergo some degree of thermalization prior to ionization. However, it is interesting to note that some of the molecules that reached 60% ionization are still quite translationally hot. This implies that a translationally hot HCl molecule has a fluctuating ionic character as it moves and changes position.

Figure 11B gives information about the number of potential candidates for proton transfer at the moment the HCl reached values of 20%, 40%, and 60% ionic character Specifically, we consider the number of (Cl)H- -O(Gly) distances that are less than a specified cutoff distance (taken to be 4 Å). We note that there tend to be many more close contacts between the hydrogen of HCl and the oxygen of glycerol as the degree of ionization is increased. This suggests that the thermalization process is correlated not only with the increased ionic character, but also with enhanced solvation structure. The thermalized HCl molecules, which are preferentially oriented with their hydrogen end pointing toward the bulk liquid, may undergo proton transfer through any one of the relatively large number of OH contacts established by the solvation process. Figure 12 quantifies this by showing the radial distribution functions of the Cl(H)−O−Gly distances. The data in this figure are obtained independently from an equilibrated covalent HCl (top panel) and HCl ion pair (bottom panel) at the Gibbs surface (thin line) and in bulk glycerol (thick line). We note that the solvation structure is much tighter around the ion pair than the covalent HCl and that the ion pair is also strongly solvated at the interface. The number of nearest neighbors (calculated from the integral of the radial distribution function to the first minimum) in the covalent state is 3.1 and 1.6 in the bulk and at the interface, respectively, while these numbers are 5.0 (bulk) and 3.4 (interface) in the ionic state. In contrast, the solvation structure around the Cl atom is much less defined and is significantly reduced at the interface relative to the bulk (data not shown).

IV. Conclusions

We have developed a simple model based on the Empirical Valence Bond (EVB) approach, which we use to describe the early events following the collision of an HCl molecule with

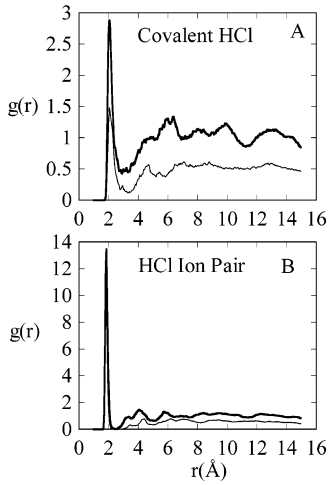

Figure 12. Pair distribution function for the hydrogen of HCl and the oxygen of glycerol for covalent (A) and contact ion pair (B) HCl molecules. In each panel the thick solid line is for HCl in the bulk and the thin solid line for HCl at the Gibbs surface.

the glycerol surface. The EVB model was parametrized by the known structure and energetics of gas-phase HCl and by the solvation thermodynamics of H^+ and Cl^- ions.

The calculated trapping probability at 2.4 and 22 kcal/mol HCl collision energies as well as the fractional energy loss of scattered HCl agree well with experiments. Collisions that give rise to scattered HCl molecules are more localized (involving fewer repulsive interactions with surface glycerol atoms) compared with collisions that lead to trapping. The trapped HCl molecule thermalizes on the picosecond time scale and begins to form a contact H^+Cl^- ion pair. The potential of mean force for HCl in bulk and surface glycerol shows a low barrier to formation of contact ion pair, suggesting the possibility of proton exchange at the interface. However, the model in its present form does not include the possibility for proton transfer to neighboring glycerol molecules. Work is in progress to investigate this feature of the HCl dissociation in glycerol.

Acknowledgment. This work has been supported by the National Science Foundation (grant CHE-9981847 to I.B. and grant CHE-9804698 to G.M.N.).

References and Notes

(1) Warshel, A.; Weiss, R. M. *J. Am. Chem. Soc.* **1980**, *102*, 6218.
(2) Hynes, J. T. The theory of reactions in solution. In *The Theory of Chemical Reactions*; Baer, M., Ed.; CRC Press: Boca Raton, FL, 1985; Vol. 4, p 171.
(3) Buesnel, R.; Miller, I. H.; Masters, A. J. *Chem. Phys. Lett.* **1995**, *247*, 391.
(4) Ando, K.; Hynes, J. T. *J. Mol. Liquids* **1995**, *64*, 25.
(5) Laria, D.; Kapral, R.; Estrin, D.; Ciccotti, G. *J. Chem. Phys.* **1996**, *104*, 6560.
(6) Ando, K.; Hynes, J. T. *J. Phys. Chem. B* **1997**, *101*, 10464.
(7) Cuma, M.; Schmitt, U. W.; Voth, G. A. *Chem. Phys.* **2000**, *258*, 187.
(8) Thompson, W. H.; Hynes, J. T. *J. Phys. Chem. A* **2001**, *105*, 2582.
(9) Buch, V.; Sadlej, J.; Aytemiz-Uras, N.; Delvin, J. P. *J. Phys. Chem. A* **2002**, *106*, 9374.
(10) Devlin, J. P.; Uras, N.; Sadlej, J.; Buch, V. *Nature* **2002**, *417*, 269.
(11) Cabaleiro-Lago, E. M.; Hermida-Ramón, J. M.; Rodríguez-Otero, J. *J. Chem. Phys.* **2002**, *117*, 3160.
(12) *The Chemistry of Acid Rain*: *Sources and Atmospheric Processes*; Johnson, R. W., Gordon, G. E., Eds.; American Chemical Society Symposium Series; American Chemical Society: Washington, DC, 1987.
(13) Ringeisen, B. R.; Muenter, A. H.; Nathanson, G. M. *J. Phys. Chem. B* **2002**, *106*, 4988.
(14) Ringeisen, B. R.; Muenter, A. H.; Nathanson, G. M. *J. Phys. Chem. B* **2002**, *106*, 4999.
(15) Hu, J. H.; Shorter, J. A.; Davidovits, P.; Worsnop, D. R.; Zahniser, M. S.; Kolb, C. E. *J. Phys. Chem.* **1993**, *97*, 11037.
(16) Nathanson, G. M.; Davidovitz, P.; Worsnop, D. R.; Kolb, C. E. *J. Phys. Chem.* **1996**, *100*, 13007.
(17) Finlayson-Pitts, B. J.; Pitts, J. N. *Chemistry of the Upper and Lower Atmospher*; Academic: New York, 2000.
(18) Danckwerts, P. V. *Gas−Liquid Reactions*; McGraw-Hill: New York, 1970; Chapter 10.
(19) Eigen, M. *Pure Appl. Chem.* **1963**, *6*, 97.
(20) Gertner, B. J.; Hynes, J. T. *Faraday Discuss. Chem. Soc.* **1998**, *110*, 301.
(21) Svanberg, M.; Pettersson, J. B. C.; Bolton, K. *J. Phys. Chem. A* **2000**, *104*, 5787.
(22) Milet, A.; Struniewicz, C.; Moszynski, R.; Wormer, P. E. S. *J. Chem. Phys.* **2001**, *115*, 349.
(23) Baldelli, S.; Schnitzer, C.; Shultz, M. J. *J. Chem. Phys.* **1998**, *108*, 9817.
(24) Baldelli, S.; Schnitzer, C.; Shultz, M. J. *Chem. Phys. Lett.* **1999**, *302*, 157.
(25) Benjamin, I.; Wilson, M. A.; Pohorille, A. *J. Chem. Phys.* **1994**, *100*, 6500.
(26) Benjamin, I.; Wilson, M. A.; Pohorille, A.; Nathanson, G. M. *Chem. Phys. Lett.* **1995**, *243*, 222.
(27) Root, L. J.; Stillinger, F. H. *J. Chem. Phys.* **1989**, *90*, 1200.
(28) Root, L. J.; Stillinger, F. H. *Phys. Rev. B* **1990**, *41*, 2348.
(29) Root, L. J.; Berne, B. J. *J. Chem. Phys.* **1999**, *107*, 4350.
(30) Chelli, R.; Procacci, P.; Cardini, G.; Valle, R. G. D.; Califano, S. *Phys. Chem. Chem. Phys.* **1999**, *1*, 871.
(31) Weiner, S. J.; Kollman, P. A.; Nguyen, D. T.; Case, D. A. *J. Comput. Chem.* **1986**, *7*, 230.
(32) Hansen, J.-P.; McDonald, I. R. *Theory of Simple Liquids*, 2nd ed.; Academic: London, UK, 1986.
(33) Lide, D. R. *Handbook of Chemistry and Physics*, 71st ed.; CRC Press: Boca Raton, FL, 1990.
(34) Huber, K. P.; Herzberg, G. *Constants of Diatomic Molecules*; Van Nostrand Reinhold: New York, 1979.
(35) Votava, C.; Ahlrichs, R.; Geiger, A. *J. Chem. Phys.* **1983**, *78*, 6841.
(36) McQuarrie, D. A. *Statistical Mechanics*; Harper & Row: New York, 1976.
(37) Allen, M. P.; Tildesley, D. J. *Computer Simulation of Liquids*; Clarendon: Oxford, UK, 1987.
(38) Benjamin, I. *Chem. Rev.* **1996**, *96*, 1449.
(39) Bentzien, J.; Muller, R. P.; Florián, J.; Warshel, A. *J. Phys. Chem. B* **1998**, *102*, 2293.
(40) Strajbl, M.; Hong, G.; Warshel, A. *J. Phys. Chem. B* **2002**, *106*, 13333.
(41) Harris, J.; Weinberg, W. H. In *Dynamics of Gas−Surface Interactions*; Rettner, C. T., Ashfold, M. N. R., Eds.; Royal Society of Chemistry: Cambridge, UK, 1991.
(42) Saecker, M. E.; Nathanson, G. M. *J. Chem. Phys.* **1993**, *99*, 7056.
(43) Garten, D. J.; K., M. T.; M., A.; Balucani, N.; P., C.; Volpi, G. G. *J. Chem. Phys.* **2001**, *114*, 5958.